DMD Fast Forward. Published on November 3, 2020 as DOI: 10.1124/dmd.120.000115
This article has not been copyedited and formatted. The final version may differ from this version.

Title

Functional investigation of solute carrier family 35, member F2 (SLC35F2) in three cellular models of the primate blood–brain barrier

Tatsuki Mochizuki*, Tadahaya Mizuno*, Toshiki Kurosawa, Tomoko Yamaguchi, Kei Higuchi, Yuma Tega, Yoshitane Nozaki, Kenji Kawabata, Yoshiharu Deguchi and Hiroyuki Kusuhara

*Equally contributed to this work

Laboratory of Molecular Pharmacokinetics, Graduate School of Pharmaceutical Sciences, The University of Tokyo, Tokyo, Japan (T.Mo., T.Mi., H.K.)

Laboratory of Drug Disposition and Pharmacokinetics, Faculty of Pharma-Sciences, Teikyo University, Tokyo, Japan (T.K., K.H., Y.T., Y.D.)

Laboratory of Stem Cell Regulation, National Institutes of Biomedical Innovation, Health and Nutrition, Osaka, Japan (T.Y., K.K.)

Department of Cell Biology and Biochemistry, Texas Tech University Health Sciences Center, Lubbock, TX, USA (K.H., current address)

Drug Metabolism and Pharmacokinetics Tsukuba, Tsukuba Research Laboratories, Eisai Co., Ltd., Tsukuba, Ibaraki, Japan (Y.N.)

DMD Fast Forward. Published on November 3, 2020 as DOI: 10.1124/dmd.120.000115
This article has not been copyedited and formatted. The final version may differ from this version.

Running title

Role of SLC35F2 in various BBB models

Address correspondence to

Hiroyuki Kusuhara, Ph.D

Professor, Laboratory of Molecular Pharmacokinetics, Graduate School of Pharmaceutical Sciences, The University of Tokyo, 7-3-1 Hongo, Bunkyo-ku, Tokyo 113-0033, Japan. Tel: +81-3-5841-4770; Fax: +81-3-5841-4766; E-mail: kusuhara@mol.f.u-tokyo.ac.jp

Manuscript metrics

Number of text pages: 34

Number of tables: 3 (+ 3 supplementary)

Number of figures: 6 (+ 8 supplementary)

Number of references: 41

Number of words in the Abstract: 250

Number of words in the Introduction: 606

Number of words in the Discussion: 1154

Abbreviations

BBB, blood–brain barrier; BCRP, breast cancer-resistant protein; BMECs, brain microvascular endothelial cells; hCMEC, human Cerebral Microvascular Endothelial Cell; CNS, central nervous system; hSLC35F2, human solute carrier family 35, member F2; iPS, induced pluripotent stem; KD, knockdown; KO, knockout; LC-MS/MS, liquid chromatography-tandem mass spectrometry; mSLC35F2, mouse solute carrier family 35, member F2; OATP, organic anion transporting polypeptide; P-gp, P-glycoprotein; SLC, solute carrier family; SLC35F2, solute carrier family 35, member F2; TEER, transendothelial electrical resistance

DMD Fast Forward. Published on November 3, 2020 as DOI: 10.1124/dmd.120.000115
This article has not been copyedited and formatted. The final version may differ from this version.

Abstract

Understanding the mechanisms of drug transport across the blood–brain barrier (BBB) is an important issue for regulating the pharmacokinetics of drugs in the central nervous system. In this study, we focused on solute carrier family 35, member F2 (SLC35F2), whose mRNA is highly expressed in the BBB. SLC35F2 protein was enriched in isolated mouse and monkey brain capillaries relative to brain homogenates and was localized exclusively on the apical membrane of MDCKII cells and brain microvascular endothelial cells (BMECs) differentiated from human induced pluripotent stem cells (hiPS-BMECs). SLC35F2 activity was assessed using its substrate, YM155, and pharmacological experiments revealed SLC35F2 inhibitors, such as famotidine (half-maximal inhibitory concentration, 160 μM). Uptake of YM155 was decreased by famotidine or SLC35F2 siRNA transfection in immortalized human BMECs (hCMEC/D3 cells). Furthermore, famotidine significantly inhibited the apical-to-basal (A-to-B) transport of YM155 in primary cultured monkey BMECs and hiPS-BMECs. Crucially, SLC35F2-knockout diminished the A-to-B transport and intracellular accumulation of YM155 in hiPS-BMECs. By contrast, in studies using an *in situ* brain perfusion technique, neither deletion of *Slc35f2* nor famotidine reduced brain uptake of YM155, even though YM155 is a substrate of mouse SLC35F2. YM155 uptake was decreased significantly by losartan and naringin, inhibitors for the organic anion transporting polypeptide 1A4 (OATP1A4). These findings suggest SLC35F2 is a functional transporter in various cellular models of the primate BBB that delivers its substrates to the brain and that its relative importance in the BBB is modified by differences in the expression of OATPs between primates and rodents.

DMD Fast Forward. Published on November 3, 2020 as DOI: 10.1124/dmd.120.000115
This article has not been copyedited and formatted. The final version may differ from this version.

Significance statement

This study demonstrated that SLC35F2 is a functional drug influx transporter in three different cellular models of the primate blood–brain barrier (i.e., hCMEC/D3 cells, primary cultured monkey BMECs, and hiPS-BMECs), but has limited roles in mouse brain. SLC35F2 facilitates apical-to-basal transport across the tight cell monolayer. These findings will contribute to the development of improved strategies for targeting drugs to the central nervous system.

DMD Fast Forward. Published on November 3, 2020 as DOI: 10.1124/dmd.120.000115
This article has not been copyedited and formatted. The final version may differ from this version.

Introduction

It is well accepted that drugs must cross the blood–brain barrier (BBB) formed by a tight monolayer of brain microvascular endothelial cells (BMECs) from the blood circulation to reach their targets in the central nervous system (CNS). Hence, understanding the mechanisms associated with drug transport across the BBB is critically important for the development of effective CNS drugs. Efflux transporters, such as P-glycoprotein (P-gp) and breast cancer-resistance protein (BCRP), have been well characterized in both preclinical animal and human BBB models, and reduce the distribution of their substrate drugs within the CNS via their transport activities (Demeule *et al.*, 2002; Sasongko *et al.*, 2005; Nicolazzo and Katneni, 2009). Moreover, many researchers have investigated transporters that can facilitate the transfer of drugs from the blood to the CNS. For instance, the function of organic anion transporting polypeptide 1A4 (OATP1A4), has been extensively investigated preclinically. However, in our previous report, convincing data were not available to support its targeting efficacy for organic anions *in vivo* (Ose *et al.*, 2010). On the other hand, the distribution of [D-penicillamine^{2,5}]-enkephalin, a substrate of OATP1A4 within the brain, was consistently altered by changes in OATP1A4 expression under normal conditions and those mimicking disease. In addition, the distribution was decreased by OATP inhibitors, suggesting a role for OATP1A4 in targeting drugs to the brain (Ronaldson *et al.*, 2011). It has also been speculated that several hydrophobic, cationic drugs such as pyrilamine, oxycodone and tramadol, can cross the BBB via a proton/organic cation antiporter(s) (Okura *et al.*, 2008; Kitamura *et al.*, 2014; Higuchi *et al.*, 2015). In another report, it was demonstrated that some D2 dopamine receptor antagonists, i.e., olanzapine, haloperidol and risperidone, displayed higher receptor occupancy in the cortex than in the human pituitary (Arakawa *et al.*, 2010). This finding suggested unknown mechanism(s) in the brain that cause higher unbound drug concentrations in the cerebral cortex than in the pituitary. These include active transporters in the BBB to delivery drugs into the CNS because these drugs can freely access their targets from the blood in the pituitary.

DMD Fast Forward. Published on November 3, 2020 as DOI: 10.1124/dmd.120.000115
This article has not been copyedited and formatted. The final version may differ from this version.

In the present study, we focused on solute carrier family 35, member F2 (SLC35F2) which is highly expressed in BMECs compared with endothelial cells in other tissues and other brain cells in mice (Daneman *et al.*, 2010; Zhang *et al.*, 2014). SLC35F2 was initially identified as a membrane protein acting as a retroviral receptor (Sarangi *et al.*, 2007). Subsequently, SLC35F2 was identified by genome-wide screening in KBM7 cells as a transporter for a Survivin inhibitor, YM155, which sensitizes KBM7 as well as various other cells to YM155 cytotoxicity (Winter *et al.*, 2014). With regard to other SLC-type transporters accepting YM155 as a substrate, OCT1 and OCT2 have been identified as candidates to account for the uptake of YM155 in xenobiotic clearance organs, such as liver and kidney, respectively (Minematsu *et al.*, 2010). In addition, YM155 is also recognized as a substrate by P-gp (Iwai *et al.*, 2011), which conferred resistance to YM155 (Radic-Sarikas *et al.*, 2017).

In the present study, we aimed to characterize SLC35F2 as a drug transporter in the BBB. To characterize SLC35F2 transport function, we constructed HEK293 cells stably expressing SLC35F2 and SLC35F2 knockout PC-3 cells (Winter *et al.*, 2014). We assessed SLC35F2 activity in three cellular models of the BBB: (i) hCMEC/D3 cells, an immortalized human BMECs (Weksler *et al.*, 2013); (ii) a cellular model of monkey BBB composed of primary cultured, monkey BMECs, rat pericytes and astrocytes; and (iii) BMECs derived from human-induced pluripotent stem cells (hiPS-BMECs) (Lippmann *et al.*, 2012, 2014; Kurosawa *et al.*, 2018). In addition, the role of SLC35F2 *in vivo* was investigated using *Slc35f2*$^{-/-}$ mice.

DMD Fast Forward. Published on November 3, 2020 as DOI: 10.1124/dmd.120.000115
This article has not been copyedited and formatted. The final version may differ from this version.

Materials and Methods

Reagents

YM155 monobromide was purchased from Funakoshi Co. (Tokyo, Japan). All other chemicals and reagents were of reagent grade and commercially available.

Cell culture

HEK293 and MDCKII cells were cultured in Dulbecco's modified Eagle's medium (low glucose; Invitrogen, Carlsbad, CA, USA) supplemented with 10% fetal bovine serum. PC-3 cells (American Type Culture Collection: CRL-1435) were cultured in RPMI1640 medium (Invitrogen) supplemented with 10% fetal bovine serum. hCMEC/D3 cells were maintained on collagen-coated dishes as reported previously (Okura *et al.*, 2014). MBT-24H (lot: 24E50), which we abbreviated as monkey BMECs, was purchased from Pharmaco-Cell Co. (Nagasaki, Japan). This model was composed of monkey BMECs and rat pericytes and astrocytes, and was maintained according to the manufacturer's protocol (Nakagawa *et al.*, 2007). Transcellular transport analysis using monkey BMECs was conducted on day 5 of the culture. The hiPS cell line (IMR90-C4; WiCell, Madison, WI, USA) was cultured in mTeSR1 medium without human fibroblast growth factor 2 (FGF2) in a Matrigel-coated dish. The differentiation to hiPS-BMECs was conducted as described previously (Lippmann *et al.*, 2012, 2014; Kurosawa *et al.*, 2018). All cells were maintained at 37 °C under an atmosphere of 5% CO_2 in air with 95% humidity.

Animals

Slc35f2$^{-/-}$ mice were established using the CRISPR/Cas9 gene knockout system in the Laboratory Animal Resource Center, University of Tsukuba (Ibaraki, Japan). Male C57BL/6J were purchased from CLEA Japan (Tokyo, Japan). All mice were maintained at a controlled temperature under a 12-h light/dark cycle. Food and water were available ad libitum. All experiments using animals in this study were performed according to the guidelines provided by the Institutional Animal Care Committee (Graduate School of Pharmaceutical Sciences, University of Tokyo, Tokyo, Japan). Monkey tissues were prepared from young, adult

DMD Fast Forward. Published on November 3, 2020 as DOI: 10.1124/dmd.120.000115
This article has not been copyedited and formatted. The final version may differ from this version.

(approximately 10 years old), nonnaïve male cynomolgus macaques (*Macaca fascicularis*) by the procedures approved by the Institutional Animal Care and Use Committee of Eisai Tsukuba Research Laboratories (Ibaraki, Japan).

Construction of SLC35F2 knockout PC-3 cells

The gene knockout in the PC-3 cells was produced using the CRISPR/Cas9 system. The CRISPR oligo sequences used are listed in Supplementary Table 1. The cell-construction method used was similar to that reported previously (Winter *et al.*, 2014) with some modifications and the details are shown in Supplementary Methods.

Isolation of crude membrane-enriched fraction of isolated brain capillaries

The protocol used to isolate crude membrane fractions of brain capillaries was as described previously (Ose *et al.*, 2010). All steps were conducted at 4 °C. Monkey specimens were derived from a single brain hemisphere and mice samples were from the whole brains of eight male mice (9–10 weeks old).

Immunoblotting analysis

Specimens were lysed using Cell Lysis Buffer (Cell Signaling Technology, Danvers, MA, USA) and reduced for 5 min at 60 °C with 40 μL of sodium lauryl sulfate (SDS) sample buffer (New England BioLabs, Beverly, MA, USA) containing 2-mercaptoethanol. Samples were loaded into wells of a 10% SDS-polyacrylamide gel with a 3.75% stacking gel, electrophoresed, and subjected to western blot analysis, as described previously (Mizuno *et al.*, 2015). SLC35F2 was detected using a 1:1000 dilution of primary antibody (HPA048185; Merck, Darmstadt, Germany).

Immunocytochemistry

HEK293 cells and PC-3 cells were seeded on glass coverslips (Matsunami Glass Industries, Osaka, Japan) in 12-well plates at a density of 1.0×10^5 cells per well for 24 h. Similarly, MDCKII cells were seeded at a density of 5.0×10^5 cells per well, and cultured for 48 h to construct a monolayer structure. MDCKII cells were transfected with pcDNA3.1(+) vector containing hSLC35F2-HA or mSLC35F2-HA at 24 h after seeding. hiPS-BMECs were

DMD Fast Forward. Published on November 3, 2020 as DOI: 10.1124/dmd.120.000115
This article has not been copyedited and formatted. The final version may differ from this version.

prepared using the same protocol as the transcellular transport assay. Immunocytochemical assays were conducted as described previously (Hayashi *et al.*, 2016). Cells were fixed in 4% paraformaldehyde/phosphate-buffered saline (PBS) for 10 min, permeabilized in 0.1% saponin/PBS for 10 min, blocked with 3% bovine serum albumin (BSA)/PBS for 30 min, followed by 2 h incubation at room temperature with primary antibodies: anti-HA (1:250, 3F10; Roche Diagnostics, Mannheim, Germany), anti-SLC35F2 (1:20, HPA048185; Merck), or anti-Na^+/K^+ ATPase (1:20, C464.6; Merck). After washing with PBS, cells were incubated with Alexa Fluor 488/546/555-conjugated secondary antibody and TO-PRO-3 (Thermo Fisher Scientific, Waltham, MA, USA) for 1 h at room temperature. Cells were mounted onto glass slides with Vectashield mounting medium (Vector Laboratories, Burlingame, CA, USA) and then visualized by confocal microscopy using a Leica TCS SP5 II laser scanning confocal microscope (Leica, Solms, Germany).

***In vitro* uptake assay**

In vitro uptake studies with HEK293, PC-3, and hCMEC/D3 cells were conducted as reported previously (Deguchi *et al.*, 2004; Tsuruya *et al.*, 2016). To determine the uptake of compounds, the cells were recovered in water using a scraper and disrupted by sonication. A threefold volume of acetonitrile was added for deproteinization, and the specimens were centrifuged for 5 min at 20,000 *g*. The protein concentration was determined using the Lowry method with BSA as the standard.

***In vitro* permeability test**

In vitro permeability tests using monkey BMECs and hiPS-BMECs were conducted as described previously (Kurosawa *et al.*, 2018). The apparent permeability coefficient (P_{app}) was calculated as follows:

$$P_{\mathrm{app}} = \frac{\mathrm{d}Q/\mathrm{d}t}{D_0 \times S},$$

where $\mathrm{d}Q/\mathrm{d}t$, D_0, and S are the slope of the linear region of the cumulative amount of permeant in the receiver chamber versus time plot, the starting concentration of the drug on the donor side, and the area of the porous membrane, respectively. Compounds

DMD Fast Forward. Published on November 3, 2020 as DOI: 10.1124/dmd.120.000115
This article has not been copyedited and formatted. The final version may differ from this version.

accumulated in the cell were collected by treatment with MeOH for 10 min at room temperature.

***In situ* brain perfusion test in mice**

In situ brain perfusion in mice was performed as described previously (Dagenais *et al.*, 2000; Ose *et al.*, 2010; Sano *et al.*, 2018) and the details are available in the Supplementary Methods.

Quantification of test compounds

Lucifer yellow was detected using an Infinite M200 spectrometer (428/536 nm; Tecan, Crailsheim, Germany) or liquid chromatography with a fluorescence detector composed of a Nexera system equipped with an RF-20Axs (Shimadzu, Kyoto, Japan). Other compounds were quantified using LC-MS/MS. A SCIEX QTRAP 5500 mass spectrometer (Applied Biosystems, Foster City, CA, USA) equipped with a Prominence LC system (Shimadzu), and operated in electrospray ionization mode was used for the analysis. The conditions are summarized in Supplementary Table 2.

Kinetic analysis of data obtained *in vitro*

The uptake in the transporter-expressing cells was subjected to the kinetic analyses without subtraction of the uptake in the mock cells. The curve fitting was conducted with the iterative nonlinear least-squares method using the MULTI program (Yamaoka *et al.*, 1981) and the damped Gauss–Newton algorithm.

The apparent kinetic parameters were estimated, assuming the Michaelis–Menten equation as follows:

$$v = \frac{V_{\mathrm{max,app}} \times \mathrm{S}}{K_{\mathrm{m,app}} + \mathrm{S}} + P_{\mathrm{dif}} \times \mathrm{S},$$

where v, $K_{\mathrm{m,\,app}}$, S, $V_{\mathrm{max,\,app}}$, P_{dif} represent the uptake velocity, Michaelis constant, substrate concentration, maximum transport velocity, and nonsaturable uptake clearance, respectively. The IC_{50} values against YM155 uptake for hSLC35F2 were calculated as follows:

$$CL_{\mathrm{uptake\ (+\ Inhibitor)}} = \frac{CL_{\mathrm{uptake\ (control)}}}{1+{}^{I}/_{\mathrm{IC_{50}}}},$$

DMD Fast Forward. Published on November 3, 2020 as DOI: 10.1124/dmd.120.000115
This article has not been copyedited and formatted. The final version may differ from this version.

where $CL_{uptake\ (+Inhibitor)}$ and $CL_{uptake\ (control)}$ represent the uptake clearance in the presence and absence of inhibitors, respectively, and *I* represents the inhibitor concentration.

Data analysis

The statistical significance of differences were determined using a Welch *t* test and one-way analysis of variance followed by a Tukey or Dunnett multiple-comparison test. Data were analyzed using Prism software (version 4.0, GraphPad Software, La Jolla, CA, USA).

DMD Fast Forward. Published on November 3, 2020 as DOI: 10.1124/dmd.120.000115
This article has not been copyedited and formatted. The final version may differ from this version.

Results

Expression of SLC35F2 in the BBB and localization in MDCKII cells

Immunoblotting analysis using anti-SLC35F2 antibody revealed that a band around 37 kDa was concentrated in the crude membrane-enriched fraction of isolated brain capillaries, compared to the corresponding fraction of brain homogenates from wild-type (WT) mice and a similar concentration was not observed in specimens from *Slc35f2*$^{-/-}$ mice (**Figure 1A**). In addition, the same size band was detected in the crude membrane-enriched fraction of isolated brain capillaries from monkey brain (**Figure 1B**).

We conducted an immunohistochemical study of SLC35F2 in a mouse brain, but specific signals associated with SLC35F2 were not detected (data not shown). In C-terminal HA-tagged, hSLC35F2 (hSLC35F2-HA) transfected MDCKII cells, which are polarized when constructing a tight cell monolayer, hSLC35F2-HA was detected mainly on the apical membrane of the cells (**Figure 1C**) and mSLC35F2-HA produced a similar result (data not shown). These data suggest the localization of SLC35F2 on the luminal membrane (corresponding to the apical membrane) in endothelial cells.

YM155 transport function mediated by hSLC35F2 and mSLC35F2

We established HEK293 cell clones stably expressing hSLC35F2-HA (hSLC35F2-HEK293) or mSLC35F2-HA (mSLC35F2-HEK293) as described in the Supplementary Methods. SLC35F2 expression was confirmed by immunoblotting (**Supplementary Figure 1A**) and immunocytochemistry (**Supplementary Figure 1B**). YM155 uptake was significantly increased in both cell lines compared with mock-transfected HEK293 cells (**Supplementary Figure 1C**). Specific YM155 uptake mediated by SLC35F2 was determined at 5 min in subsequent analysis, as the initial uptake velocities were maintained during this time. The concentration dependency of YM155 uptake is illustrated as Eadie–Hofstee plots (**Supplementary Figure 1D**) and the calculated kinetic parameters displayed little species difference (**Table 1**). The uptake curve extrapolated to time zero did not pass through the

DMD Fast Forward. Published on November 3, 2020 as DOI: 10.1124/dmd.120.000115
This article has not been copyedited and formatted. The final version may differ from this version.

origin, suggesting that our analysis of uptake velocity may have underestimated the initial uptake velocity. Thus, the kinetic parameters represent apparent values.

Effect of organic cations on YM155 uptake facilitated by SLC35F2 in PC-3 cells

YM155 uptake was detected even in mock-transfected HEK293 cells (about 60 μL/5 min/mg protein), accounting for 27% of the uptake in hSLC35F2-HEK293 (**Supplementary Figure 1C**). To evaluate the specific hSLC35F2 activity more precisely, we constructed SLC35F2 knockout cells using PC-3 cells that express high endogenous levels of hSLC35F2 (Winter *et al.*, 2014). Depletion of SLC35F2 was confirmed by immunoblotting and immunocytochemistry analysis (**Supplementary Figure 2A**, **B**), and the SLC35F2 deficiency dramatically decreased YM155 uptake activity to 10% of control cells (**Table 2**).

In studies to characterize SLC35F2-mediated transport, the effects of various organic cations on YM155 uptake were examined in PC-3 cells (**Table 2**). Some of the selected compounds were reported to inhibit the function of organic cation transporters. For example, L-carnitine has been shown to inhibit the organic cation/carnitine transporters (OCTNs), and tetraethylammonium (TEA) inhibits organic cation transporters (OCTs) (Koepsell *et al.*, 2007). In contrast to their effect on these transporters, L-carnitine and TEA had no effect or only a small effect on YM155 uptake mediated by SLC35F2. By contrast, other drugs did inhibit SLC35F2-mediated transport, and the results for some compounds were consistent with a previous report (Minematsu *et al.*, 2009). Apart from famotidine, all the effective drugs were shown to inhibit the unknown proton/organic cation (H^+/OC) antiporter(s), reported to be functional in the BBB (Okura *et al.*, 2008; Kitamura *et al.*, 2014; Suzuki *et al.*, 2016; Kurosawa *et al.*, 2017). To determine their relative inhibitory potency, we calculated half-maximal inhibitory concentration values for famotidine, clonidine, diphenhydramine, pyrilamine, imipramine, and quinidine (**Table 3**; **Supplementary Figure 3**).

Investigation of SLC35F2 substrates other than YM155

To examine whether SLC35F2 transports various xenobiotics, we conducted uptake studies in two cellular models: mock-transfected HEK293 cells versus mSLC35F2-HEK293 cells, and

DMD Fast Forward. Published on November 3, 2020 as DOI: 10.1124/dmd.120.000115
This article has not been copyedited and formatted. The final version may differ from this version.

control versus SLC35F2 knockout PC-3 cells. Among the tested compounds, only the uptake of famotidine was significantly altered in both cellular models (**Supplementary Figure 4A**). Famotidine uptake was significantly inhibited by excess YM155 in mSLC35F2-HEK293 cells (**Supplementary Figure 4B**), consistent with SLC35F2-mediated uptake.

Compounds that suppressed YM155 uptake in PC-3 cells included many hydrophobic cationic drugs (**Table 2**), which are easily accumulated intracellularly and thereby possibly affect the intracellular YM155 distribution to acidic subcellular organelles such as lysosomes (Kubo *et al.*, 2016). Among the SLC35F2 inhibitors studied, famotidine was identified as a novel substrate of SLC35F2 (**Supplementary Figure 4B**), which acts as a competitive inhibitor. Therefore, we used famotidine as an inhibitor for SLC35F2 in subsequent analyses.

Characterization of YM155 uptake in hCMEC/D3 cells

To investigate whether the activity of SLC35F2 is maintained in the BBB, we conducted a functional analysis with hCMEC/D3 cells, which are an immortalized cell line of human BMECs (Weksler *et al.*, 2005; Shimomura *et al.*, 2013). To characterize YM155 uptake in hCMEC/D3 cells, the time course and concentration dependency of YM155 uptake were investigated in hCMEC/D3 cells (**Figure 2A, B**; **Table 1**). The $K_{m,\,app}$ in hCMEC/D3 cells (0.57 μM) was close to that of hSLC35F2 (0.31 μM, **Table 1**), while the affinity for other YM155 transporters was 22.1 μM for OCT1 and 2.67 μM for OCT2 (Minematsu *et al.*, 2010). The profile of inhibitory effects on YM155 uptake in hCMEC/D3 cells was similar to that in PC-3 cells (**Table 2**). We also examined the effect on YM155 uptake of SLC35F2 knockdown by siRNA treatment. SLC35F2 protein expression was diminished in the whole lysate specimen of SLC35F2 siRNA-treated cells (**Figure 2C**). The fraction of YM155 uptake inhibited by famotidine (i.e., the difference in uptake between famotidine treated and non-treated conditions) was decreased by 64% by SLC35F2 knockdown, supporting the significance of SLC35F2 in YM155 uptake in hCMEC/D3 cells (**Figure 2D**).

DMD Fast Forward. Published on November 3, 2020 as DOI: 10.1124/dmd.120.000115
This article has not been copyedited and formatted. The final version may differ from this version.

The A-to-B transcellular transport of YM155 across monkey BMECs

hCMEC/D3 cells do not form a tight monolayer, which limits their application to study the directional transport of YM155 mediated by SLC35F2 (Srinivasan *et al.*, 2015). Therefore, we employed a commercial cellular model of the primate BBB, i.e., monkey BMECs (MBT-24H). SLC35F2 mRNA expression in monkey BMECs was confirmed by polymerase chain reaction (PCR) analysis (**Figure 3A**). The transendothelial electrical resistance (TEER) was above 330 $\Omega \times cm^2$ in all samples. In addition, we measured the amounts of transported lucifer yellow as a paracellular transport marker (**Supplementary Figure 5A**). In the presence of 10 μM lucifer yellow, transport levels (25–35 pmol/4 h) were low compared to those (~480 pmol/4 h) in other cellular models of the BBB, such as hCMEC/D3 and bEnd3 cells (Eigenmann *et al.*, 2013; Yang *et al.*, 2018). Therefore, we concluded that monkey BMECs can form a tight junction.

Drug transporter function in monkey BMECs was also confirmed by directional transport of quinidine, a typical reference substrate of P-gp, the B-to-A transport of which was greater than the A-to-B transport because of active efflux by P-gp in the apical membrane (Kurosawa *et al.*, 2018) (**Supplementary Figure 5B**). Likewise, the amount of YM155 B-to-A transport was about threefold higher than its apical-to-basal (A-to-B) transport (data not shown). In regard to YM155 A-to-B transport, the amount was significantly decreased by 1 mM famotidine (**Figure 3B**). In addition, the intracellular accumulation of YM155 was suppressed by famotidine from 0.03 pmol/well to an undetectable level ($\leq$0.02 pmol/well) (**Figure 3C**).

Characterization of YM155 transcellular transport in hiPS-BMECs

Recently, hiPS-BMECs were established as an emerging cellular model of the human BBB (Lippmann *et al.*, 2012, 2014). Subsequently, we demonstrated that hiPS-BMECs express various transporters and demonstrated directional transport of nutrients and prazosin across a tight cell monolayer (Kurosawa *et al.*, 2018). In the current study, we found that SLC35F2 protein expression was induced during the differentiation process, and achieved a higher

DMD Fast Forward. Published on November 3, 2020 as DOI: 10.1124/dmd.120.000115
This article has not been copyedited and formatted. The final version may differ from this version.

level than that observed in hCMEC/D3 cells (**Figure 4A**). Lucifer yellow transport in hiPS-BMECs was small, even compared with that in monkey BMECs, indicating that paracellular transport was strictly regulated in hiPS-BMECs (**Supplementary Figure 5A**, **6A**). As a control for transcellular transport, B-to-A directional transport of dantrolene, a typical BCRP substrate (Enokizono *et al.*, 2008), was confirmed as reported (Kurosawa *et al.*, 2018) (**Supplementary Figure 6B**).

A clear A-to-B directional transport of YM155 was observed, which was markedly suppressed by 1 mM famotidine (**Figure 4B**). Along with inhibition of the directional transport (**Figure 4C**), famotidine significantly suppressed YM155 intracellular accumulation (**Figure 4D**), whereas other test compounds, including TEA for OCTs, L-carnitine for OCTNs, thiamine for OCTs and thiamine transporters (SLC19A2, SLC19A3), and L-arginine for cationic amino acid transporter 1 (SLC7A1), did not affect the A-to-B transport or intracellular accumulation of YM155 (**Figure 4C**, **D**).

YM155 transcellular transport in SLC35F2 knockout hiPS-BMECs

To elucidate the role of SLC35F2 directly in hiPS-BMECs, we constructed a SLC35F2 knockout IMR90-C4 cell clone and conducted several assays after differentiation to SLC35F2 knockout hiPS-BMECs. Firstly, the absence of SLC35F2 protein was confirmed in SLC35F2 knockout hiPS-BMECs (**Figure 5A**). Using this cell as a negative control, specific SLC35F2 signal was confirmed on the apical membrane of hiPS-BMECs (**Figure 5B**, **C**). The low permeability of lucifer yellow was maintained in SLC35F2 knockout hiPS-BMECs, although the absolute values were slightly increased compared with those in control cells (**Supplementary Figure 7A**). Thus, SLC35F2 knockout apparently does not affect BCRP protein expression and transport activity in hiPS-BMECs (**Figure 5A**; **Supplementary Figure 7B**).

The A-to-B permeability of YM155 was dramatically decreased in SLC35F2 knockout hiPS-BMECs (**Figure 5D**). The permeability coefficient and the intracellular accumulation in SLC35F2 knockout hiPS-BMECs were decreased to approximately 2% and 3% of the corresponding values in the control cells, respectively (**Figure 5E**, **F**), indicating the

DMD Fast Forward. Published on November 3, 2020 as DOI: 10.1124/dmd.120.000115
This article has not been copyedited and formatted. The final version may differ from this version.

predominant contribution of SLC35F2 to the uptake of YM155 from the apical side. Notably, these results were reproduced in another clone of SLC35F2 knockout hiPS-BMECs (data not shown).

Characterization of YM155 transport across the mouse BBB

Subsequently, we examined the function of SLC35F2 *in vivo* . Because YM155 transport was confirmed for mSLC35F2 (**Table 1**), we conducted an *in situ* brain perfusion test to characterize the BBB transport of YM155 in mice. In WT mice, the apparent volume of brain distribution (V_{brain}) of YM155 was decreased according to the concentration in the perfusate (**Figure 6A**), which suggests that uptake into the brain from the perfusate or the tissue binding of YM155 was saturated. However, the V_{brain} of YM155 was unchanged by *Slc35f2* deletion (**Figure 6B**) or famotidine (**Figure 6C**). Instead, we discovered that losartan and naringin, which are inhibitors for the OATP family (Rebello *et al.*, 2012; De Bruyn *et al.*, 2013), significantly suppressed the V_{brain} of YM155 (**Figure 6D**). Similarly, the V_{brain} of pitavastatin, the permeability of which across the BBB is determined by OATP1A4 (Ose *et al.*, 2010), was significantly decreased by these inhibitors.

To further explore this possibility, the uptake of YM155 was determined in HEK293 cells expressing mouse OATP1A4 and human OATP1A2, the human ortholog of OATP1A4. Both types of cells displayed significant YM155 uptake (**Supplementary Figure 8A**, **B**). The uptake mediated by mouse OATP1A4 was saturable with a $K_{m,\,app}$ value of 5.81 $\pm$ 0.99 μM (data not shown).

DMD Fast Forward. Published on November 3, 2020 as DOI: 10.1124/dmd.120.000115
This article has not been copyedited and formatted. The final version may differ from this version.

Discussion

In the development of drugs for treating brain diseases, their successful passage through the BBB is one of the critical factors. Therefore, understanding transport mechanisms for drugs at the BBB is of great importance. In the present study, we aimed to investigate the significance of SLC35F2 as a drug transporter within the BBB.

Immunoblotting clearly demonstrated the abundant expression of SLC35F2 in the isolated mouse and monkey BBB fraction compared with levels in the brain (**Figure 1A**, **B**). We also found that SLC35F2 expression was highly induced in hiPS-BMECs compared with levels in hiPS (**Figure 4A**). To identify the direction of SLC35F2-mediated transport across the BBB, identifying the membrane localization of SLC35F2 is essential. We observed that hSLC35F2 was predominantly localized in the apical membrane of MDCKII cells transfected with hSLC35F2-HA (**Figure 1C**), and of hiPS-BMECs (**Figure 5B**), but we could not successfully detect specific SLC35F2 staining in mouse brain by immunohistochemistry (data not shown). Endothelial cells are polarized cells and their apical membrane is exposed to the blood *in vivo* ; therefore, it is reasonable that active efflux transporters such as P-gp and BCRP, which are located on the apical membrane, limit the distribution of their substrates from the circulation into the CNS (Demeule *et al.*, 2002; Sasongko *et al.*, 2005; Nicolazzo and Katneni, 2009). As SLC35F2 is also predominantly expressed in the apical membrane, it is likely to facilitate the blood-to-brain transport of its substrates. Indeed, a series of *in vitro* studies using famotidine or SLC35F2 knockdown or knockout in three cellular models of the primate BBB support the crucial role of SLC35F2 in YM155 uptake (**Figures 2D, 3C, 4F**). Furthermore, in the BBB models which form tight monolayers, SLC35F2-mediated uptake of YM155 was remarkable from the apical side, and thereby facilitated the apical-to-basal transport across the monolayer (**Figures 3B, 5D, E**).

We found a discrepancy in the dominant direction in the transcellular transport of YM155 between monkey BMECs and hiPS-BMECs. The B-to-A transport was greater than the A-to-B transport in monkey BMECs, but was vice versa in hiPS-BMECs. YM155 is a

DMD Fast Forward. Published on November 3, 2020 as DOI: 10.1124/dmd.120.000115
This article has not been copyedited and formatted. The final version may differ from this version.

substrate of P-gp (Iwai *et al.*, 2011); therefore, it is reasonable to assume P-gp played a role in limiting the A-to-B transport of YM155 and in facilitating the B-to-A transport in the BBB, as observed for other P-gp substrates (Mizuno *et al.*, 2003). Monkey BMECs obviously retain P-gp activity (**Supplementary Figure 5B**), whereas hiPS-BMECs lack P-gp (Kurosawa *et al.*, 2018). In addition, because YM155 is a water-soluble compound with poor permeability across lipid membranes without transporters (**Figure 5D**), it is also possible that other transporters contribute to the transcellular transport across monolayers, such as uptake and efflux across the basolateral membrane.

Among the models tested, monkey primary BMECs appear to be the cellular model of the BBB that is most relevant to the BBB *in vivo* , in terms of the tightness and activities of transporters. However, we observed batch differences in the quality of this model. Among those tested, lot 24E50, in which we detected the famotidine sensitivity of YM155 A-to-B transport (**Figure 3B**), displayed the highest TEER (above 330 $\Omega \times cm^2$) and the lowest lucifer yellow paracellular transport (25–35 pmol/4 h, **Supplementary Figure 5A**). The famotidine sensitivity of YM155 A-to-B transport paralleled the level of lucifer yellow transport and the B-to-A/A-to-B ratio of quinidine, which could be employed as a biomarker for the tightness of endothelial cells and the activities of transporters in this system (**Supplementary Table 3**). There remains room for improvement of this model for use in drug transport studies.

Contrary to expectations based on *in vitro* data, an *in situ* brain perfusion test in mice elucidated a limited contribution of SLC35F2 to YM155 uptake by the brain, although YM155 is a substrate of mouse SLC35F2 (**Figure 6B**, **C**). Instead, YM155 transport was likely mediated by OATP1A4 (**Figure 6D; Table 1**; **Supplementary Figure 8B**). Previously, we reported a species difference between OATP1A4 and OATP1A2 in their specificities toward cationic substrates, triptans, and sulpiride (Liu *et al.*, 2015; Sano *et al.*, 2018). However, YM155 was transported by OATP1A2. It should be noted that, unlike rodent OATP1A4, OATP1A2 protein expression levels were fairly low or undetectable in the human BBB (Uchida *et al*., 2011; Billington *et al*., 2019). As a homolog of OATP1A2, OATP2B1 protein was detectable in the human BBB by LC-MS/MS analysis (Billington *et al*., 2019). We could

DMD Fast Forward. Published on November 3, 2020 as DOI: 10.1124/dmd.120.000115
This article has not been copyedited and formatted. The final version may differ from this version.

not detect any specific uptake of YM155 by this transporter (data not shown). These results suggest the possibility of species differences between rodents and primates in the transporters responsible for YM155 transport across the BBB, due to the abundance of OATP1As. Direct demonstration of the significance of SLC35F2 in YM155 transport across the *in vivo* primate BBB remains a challenge. However, ^{11}C-labeled YM155 was recently reported as a positron emission tomography probe for assessing *in vivo* tissue distribution (Murakami *et al.*, 2013); therefore, identification of an *in vivo* inhibitor for SLC35F2 will be required to achieve this goal.

The present study highlighted SLC35F2 as a drug transporter in the BBB that can facilitate blood-to-CNS drug transport in three different cellular models of the primate BBB, although the *in vivo* relevance of this transporter needs to be examined in future studies. Other than YM155, we could only identify famotidine as a SLC35F2 substrate (**Supplementary Figure 4A**, **B**). Based on our studies, the substrate specificity appears to be narrower than the well-characterized organic cation transporters such as OCT1 and OCT2. SLC35F2 displayed a similar inhibition profile to the H^+/OC antiporter (**Table 2**) (Okura *et al.*, 2008; Kitamura *et al.*, 2014; Kurosawa *et al.*, 2017); however, SLC35F2 did not facilitate the uptake of reported H^+/OC antiporter substrates, such as clonidine and nicotine (**Supplementary Figure 4A**). Moreover, it was unlikely that YM155 transport mediated by SLC35F2 coupled with the proton gradient (**Supplementary Figure 4C**). These data suggest SLC35F2 is not an entity of the H^+/OC antiporter for hydrophobic organic cations. Because of the species difference in the transporter responsible for the BBB permeability of YM155, we deduced that YM155 functions as an organic anion transporter. However, none of the OAT and OATP substrates, including folic acid, estrone-3-sulfate, and hippuric acid, were transported by SLC35F2 (data not shown). A nutrition transporter, SLC19A3, was originally identified as a transporter for thiamine that accept drugs as substrates (Liang *et al*., 2015). SLC35F2 may serve as a transporter for essential compounds in the CNS under normal and/or diseased conditions. Considering the future applications for CNS drug delivery, extensive studies are required to elucidate the substrate recognition profile of SLC35F2.

DMD Fast Forward. Published on November 3, 2020 as DOI: 10.1124/dmd.120.000115
This article has not been copyedited and formatted. The final version may differ from this version.

In conclusion, the present study demonstrated that SLC35F2 is a functional drug transporter in the BBB and that it facilitates YM155 uptake and A-to-B transport in various cellular models of the primate BBB. Our findings contribute to an improved understanding of the drug transport mechanisms in the BBB and to the construction of better drug development strategies for brain targeting or avoiding CNS side effects.

DMD Fast Forward. Published on November 3, 2020 as DOI: 10.1124/dmd.120.000115
This article has not been copyedited and formatted. The final version may differ from this version.

Author contributions

Participated in research design: Mochizuki, Mizuno, and Kusuhara.

Conducted experiments: Mochizuki, Kurosawa, Yamaguchi, Higuchi and Tega.

Contributed new reagents or analytic tools: Kurosawa, Yamaguchi, Higuchi, Tega, Nozaki, Kawabata and Deguchi.

Performed data analysis: Mochizuki.

Wrote or contributed to the writing of the manuscript: Mochizuki, Mizuno and Kusuhara

DMD Fast Forward. Published on November 3, 2020 as DOI: 10.1124/dmd.120.000115
This article has not been copyedited and formatted. The final version may differ from this version.

References

Arakawa R, Okumura M, Ito H, Takano A, Takahashi H, Takano H, Maeda J, Okubo Y, and Suhara T (2010) Positron emission tomography measurement of dopamine D2 receptor occupancy in the pituitary and cerebral cortex: Relation to antipsychotic-induced hyperprolactinemia. *J Clin Psychiatry* **71**:1131–1137.

Dagenais C, Rousselle C, Pollack GM, and Scherrmann JM (2000) Development of an in situ mouse brain perfusion model and its application to mdr1a P-glycoprotein-deficient mice. *J Cereb Blood Flow Metab* **20**:381–386.

Daneman R, Zhou L, Agalliu D, Cahoy JD, Kaushal A, and Barres BA (2010) The mouse blood-brain barrier transcriptome: A new resource for understanding the development and function of brain endothelial cells. *PLoS One* **5**:e13741.

De Bruyn T, van Westen GJP, Ijzerman AP, Stieger B, de Witte P, Augustijns PF, and Annaert PP (2013) Structure-based identification of OATP1B1/3 inhibitors. *Mol Pharmacol* **83**:1257–1267.

Deguchi T, Kusuhara H, Takadate A, Endou H, Otagiri M, and Sugiyama Y (2004) Characterization of uremic toxin transport by organic anion transporters in the kidney. *Kidney Int* **65**:162–174.

Demeule M, Régina A, Jodoin J, Laplante A, Dagenais C, Berthelet F, Moghrabi A, and Béliveau R (2002) Drug transport to the brain: key roles for the efflux pump P-glycoprotein in the blood-brain barrier. *Vascul Pharmacol* **38**:339–348.

Eigenmann DE, Xue G, Kim KS, Moses A V., Hamburger M, and Oufir M (2013) Comparative study of four immortalized human brain capillary endothelial cell lines, hCMEC/D3, hBMEC, TY10, and BB19, and optimization of culture conditions, for an in vitro blood-brain barrier model for drug permeability studies. *Fluids Barriers CNS* **10**:33.

Enokizono J, Kusuhara H, Ose A, Schinkel AH, and Sugiyama Y (2008) Quantitative investigation of the role of breast cancer resistance protein (Bcrp/Abcg2) in limiting brain and testis penetration of xenobiotic compounds. *Drug Metab Dispos* **36**:995–1002, United States.

Hayashi H, Naoi S, Hirose Y, Matsuzaka Y, Tanikawa K, Igarashi K, Nagasaka H, Kage M, Inui A, and Kusuhara H (2016) Successful treatment with 4-phenylbutyrate in a patient with benign recurrent intrahepatic cholestasis type 2 refractory to biliary drainage and bilirubin absorption. *Hepatol Res* **46**:192–200.

Higuchi K, Kitamura A, Okura T, and Deguchi Y (2015) Memantine transport by a proton-coupled organic cation antiporter in hCMEC/D3 cells, an in vitro human blood-brain barrier model. *Drug Metab Pharmacokinet* **30**:182–187.

Iwai M, Minematsu T, Li Q, Iwatsubo T, and Usui T (2011) Utility of P-glycoprotein and organic cation transporter 1 double-transfected LLC-PK1 cells for studying the interaction of YM155 monobromide, novel small-molecule survivin suppressant, with P-glycoprotein. *Drug Metab Dispos* **39**:2314–2320.

Kitamura A, Higuchi K, Okura T, and Deguchi Y (2014) Transport characteristics of tramadol in the blood-brain barrier. *J Pharm Sci* **103**:3335–3341.

Koepsell H, Lips K, and Volk C (2007) Polyspecific organic cation transporters: structure, function, physiological roles, and biopharmaceutical implications. *Pharm Res* **24**:1227–1251.

Kubo Y, Seko N, Usui T, Akanuma S, and Hosoya K (2016) Lysosomal trapping Is present in retinal capillary endothelial cells : Insight into its influence on cationic drug transport at the inner blood – retinal barrier. *Biol Pharm Bull* **39**:1319–1324.

Kurosawa T, Higuchi K, Okura T, Kobayashi K, Kusuhara H, and Deguchi Y (2017) Involvement of proton-coupled organic cation antiporter in varenicline transport at blood-brain barrier of rats and in human brain capillary endothelial cells. *J Pharm Sci* **106**:2576–2582.

Kurosawa T, Tega Y, Higuchi K, Yamaguchi T, Nakakura T, Mochizuki T, Kusuhara H, Kawabata K, and Deguchi Y (2018) Expression and functional characterization of drug transporters in brain microvascular endothelial cells derived from human induced pluripotent stem cells. *Mol Pharm* **15**:5546–5555.

Lippmann ES, Al-Ahmad A, Azarin SM, Palecek SP, and Shusta E V. (2014) A retinoic acid-enhanced, multicellular human blood-brain barrier model derived from stem cell sources. *Sci Rep* **4**:4160.

Lippmann ES, Azarin SM, Kay JE, Nessler RA, Wilson HK, Al-Ahmad A, Palecek SP, and Shusta E V. (2012) Derivation of blood-brain barrier endothelial cells from human pluripotent stem cells. *Nat Biotechnol* **30**:783–791.

Liu H, Yu N, Lu S, Ito S, Zhang X, Prasad B, He E, Lu X, Li Y, Wang F, Xu H, An G, Unadkat JD, Kusuhara H, Sugiyama Y, and Sahi J (2015) Solute carrier family of the organic anion-transporting polypeptides 1A2- Madin-Darby canine kidney II: a promising in vitro system to understand the role of organic anion-transporting polypeptide 1A2 in blood-brain barrier drug penetration. *Drug Metab Dispos* **43**:1008–1018.

Minematsu T, Iwai M, Sugimoto K, Shirai N, Nakahara T, Usui T, and Kamimura H (2009) Carrier-mediated uptake of 1-(2-methoxyethyl)-2-methyl-4,9-dioxo-3- (pyrazin-2-ylmethyl)-4,9-dihydro-1H-naphtho[2,3-d]imidazolium bromide (YM155 monobromide), a novel small-molecule survivin suppressant, into human solid tumor and lymphoma cells. *Drug Metab Dispos* **37**:619–628.

Minematsu T, Iwai M, Usui K, Umehara T, and Kaminuma H (2010) Characterization of human organic cation transporter 1 (OCT1 / SLC22A1) - and OCT2 (SLC22A2) -mediated transport of 1-(2-methoxyethyl)-2-methyl-4,9-dioxo-3- (pyrazin-2-ylmethyl)-4,9-dihydro-1H-naphtho[2,3-d]imidazolium bromide (YM155 monobromide), a novel small molecule survivin suppressant. *Drug Metab Dispos* **38**:1–4.

Mizuno N, Niwa T, Yotsumoto Y, and Sugiyama Y (2003) Impact of drug transporter studies on drug discovery and development. *Pharmacol Rev* **55**:425–461.

Mizuno T, Hayashi H, and Kusuhara H (2015) Cellular cholesterol accumulation facilitates ubiquitination and lysosomal degradation of cell surface-resident ABCA1. *Arterioscler Thromb Vasc Biol* **35**:1347–1356.

Murakami Y, Matsuya T, Kita A, Yamanaka K, Noda A, Mitsuoka K, Nakahara T, Miyoshi S, and Nishimura S (2013) Radiosynthesis, biodistribution and imaging of [11C]YM155, a novel survivin suppressant, in a human prostate tumor-xenograft mouse model. *Nucl Med Biol* **40**:221–226.

Nakagawa S, Deli MA, Nakao S, Honda M, Hayashi K, Nakaoke R, Kataoka Y, and Niwa M (2007) Pericytes from brain microvessels strengthen the barrier integrity in primary cultures of rat brain endothelial cells. *Cell Mol Neurobiol* **27**:687–694.

Nicolazzo JA, and Katneni K (2009) Drug transport across the blood-brain barrier and the impact of breast cancer resistance protein (ABCG2). *Curr Top Med Chem* **9**:130–147.

Okura T, Hattori A, Takano Y, Sato T, Hammarlund-Udenaes M, Terasaki T, and Deguchi Y (2008) Involvement of the pyrilamine transporter, a putative organic cation transporter, in blood-brain barrier transport of oxycodone. *Drug Metab Dispos* **36**:2005–2013.

Okura T, Kato S, and Deguchi Y (2014) Functional expression of organic cation/carnitine transporter 2 (OCTN2/SLC22A5) in human brain capillary endothelial cell line hCMEC/D3, a human blood-brain barrier model. *Drug Metab Pharmacokinet* **29**:69–74.

Ose A, Kusuhara H, Endo C, Tohyama K, Miyajima M, Kitamura S, and Sugiyama Y (2010) Functional characterization of mouse organic anion transporting peptide 1a4 in the uptake and efflux of drugs across the blood-brain barrier. *Drug Metab Dispos* **38**:168–176.

Radic-Sarikas B, Halasz M, Huber KVM, Winter GE, Tsafou KP, Papamarkou T, Brunak S, Kolch W, and Superti-Furga G (2017) Lapatinib potentiates cytotoxicity of YM155 in neuroblastoma via inhibition of the ABCB1 efflux transporter. *Sci Rep* **7**:3091.

Rebello S, Zhao S, Hariry S, Dahlke M, Alexander N, Vapurcuyan A, Hanna I, and Jarugula V (2012) Intestinal OATP1A2 inhibition as a potential mechanism for the effect of grapefruit juice on aliskiren pharmacokinetics in healthy subjects. *Eur J Clin Pharmacol* **68**:697–708.

Sano Y, Mizuno T, Mochizuki T, Uchida Y, Umetsu M, Terasaki T, and Kusuhara H (2018) Evaluation of organic anion transporter 1A2-knockin mice as a model of human blood-brain barrier. *Drug Metab Dispos* **46**:1767–1775.

Sarangi A, Bupp K, and Roth MJ (2007) Identification of a retroviral receptor used by an envelope protein derived by peptide library screening. *Proc Natl Acad Sci U S A* **104**:11032–7.

Sasongko L, Link JM, Muzi M, Mankoff DA, Yang X, Collier AC, Shoner SC, and Unadkat JD (2005) Imaging P-glycoprotein transport activity at the human blood-brain barrier with positron emission tomography. *Clin Pharmacol Ther* **77**:503–514.

Shimomura K, Okura T, Kato S, Couraud P-O, Schermann J-M, Terasaki T, and Deguchi Y (2013) Functional expression of a proton-coupled organic cation (H+/OC) antiporter in human brain capillary endothelial cell line hCMEC/D3, a human blood-brain barrier model. *Fluids Barriers CNS* **10**:8.

Srinivasan B, Kolli AR, Esch MB, Abaci HE, Shuler ML, and Hickman JJ (2015) TEER measurement techniques for in vitro barrier model systems. *J Lab Autom* **20**:107–126.

Suzuki T, Aoyama T, Suzuki N, Kobayashi M, Fukami T, Matsumoto Y, and Tomono K (2016) Involvement of a proton-coupled organic cation antiporter in the blood–brain barrier transport of amantadine. *Biopharm Drug Dispos* **37**:323–35.

Tsuruya Y, Kato K, Sano Y, Imamura Y, Maeda K, Kumagai Y, Sugiyama Y, and Kusuhara H (2016) Investigation of endogenous compounds applicable to drug-drug interaction studies involving the renal organic anion transporters, OAT1 and OAT3, in humans. *Drug Metab Dispos* **44**:1925–1933.

Weksler B, Romero IA, and Couraud P-O (2013) The hCMEC/D3 cell line as a model of the human blood brain barrier. *Fluids Barriers CNS* **10**:16.

Weksler BB, Subileau EA, Holloway K, Leveque M, Nicotra A, Bourdoulous S, Turowski P, Male DK, Roux F, Greenwood J, Romero IA, Couraud PO, Hall W, Keynes M, Kingdom U, Kingdom U, and Couraud PO (2005) Blood-brain barrier-specific properties of a human adult brain endothelial cell line. *FASEB J* **19**:1872–1874.

Winter GE, Radic B, Mayor-Ruiz C, Blomen V a, Trefzer C, Kandasamy RK, Huber KVM, Gridling M, Chen D, Klampfl T, Kralovics R, Kubicek S, Fernandez-Capetillo O, Brummelkamp TR, and Superti-Furga G (2014) The solute carrier SLC35F2 enables YM155-mediated DNA damage toxicity. *Nat Chem Biol* **10**:768–773.

Yamaoka K, Tanigawa Y, Nakagawa T, and Uno T (1981) A pharmacokinetic analysis program (MULTI) for microcomputer. *J Pharmacobiodyn* **4**:879–885.

Yang S, Jin H, and Zhao Z (2018) Paracellular tightness and the functional expression of efflux transporters P-gp and BCRP in bEnd3 cells. *Neurol Res* **40**:644–649.

Zhang Y, Chen K, Sloan SA, Bennett ML, Scholze AR, O'Keeffe S, Phatnani HP, Guarnieri P, Caneda C, Ruderisch N, Deng S, Liddelow SA, Zhang C, Daneman R, Maniatis T, Barres

BA, and Wu JQ (2014) An RNA-sequencing transcriptome and splicing database of glia, neurons, and vascular cells of the cerebral cortex. *J Neurosci* **34**:11929–11947.

Conflict of interest statement

The authors declare no conflict of interest.

DMD Fast Forward. Published on November 3, 2020 as DOI: 10.1124/dmd.120.000115
This article has not been copyedited and formatted. The final version may differ from this version.

Footnotes

This study is supported by a Grant-in-Aid for Scientific Research (B) [Grant 26293032] and a Grant-in-Aid for JSPS Fellows [Grant 20J14855] from the Japanese Ministry of Education, Culture, Sports and Sciences.

DMD Fast Forward. Published on November 3, 2020 as DOI: 10.1124/dmd.120.000115
This article has not been copyedited and formatted. The final version may differ from this version.

Figure legends

Figure 1. SLC35F2 expression in the BBB and intracellular localization in MDCKII cells. (A), (B) Immunoblotting to confirm protein expression of mouse (A) and monkey (B) SLC35F2 in brain homogenate (Brain) and crude membrane fractions of brain capillaries (BBB). KO represents *Slc35f2*$^{-/-}$ mice specimens and WT represents wild-type mice specimens. P-glycoprotein (P-gp) was detected as a marker of the crude membrane fractions of BMECs. (C) hSLC35F2-HA localization in MDCKII cells detected by confocal laser scanning microscopy. Green and red fluorescence represent HA tag and Na^+/K^+ ATPase (basolateral membrane marker), respectively. The upper section illustrates the horizontal image and the lower section, the vertical image. Scale bars represent 10 μm. The experiments were repeated at least twice.

Figure 2. YM155 uptake mediated by hSLC35F2 in hCMEC/D3 cells. (A) Time course of YM155 (0.1 μM) uptake in parent hCMEC/D3 cells. (B) Eadie–Hofstee plots for 5 min of YM155 uptake in hCMEC/D3 cells. The line represents fitted curves. Details described in Materials and Methods. The plots were accounted for by a saturable and nonsaturable component. The fitted $K_{m,\,app}$, $V_{max,\,app}$, and P_{dif} calculated were shown in **Table.1**. (C), (D) Effects of SLC35F2 siRNA on YM155 uptake in hCMEC/D3 cells. Cells were treated with 10 nM negative control or SLC35F2 siRNA using Lipofectamine RNAiMAX for 48 h. (C) Immunoblotting of hCMEC/D3 whole cell lysate to investigate endogenous SLC35F2 expression and 10 nM SLC35F2 siRNA efficiency. (D) The uptake of YM155 (0.1 μM) was measured for 5 min. Open bars illustrate the results under no inhibitor-treated conditions, and the gray bars indicate the results under 1 mM famotidine-treated conditions. The error bars represent the standard error of the mean (n = 4, mean ± SE). ***$p < 0.001$ vs. control without inhibitor. $^{\#}p < 0.05$ vs. SLC35F2 KD without inhibitor. The experiments were repeated at least twice.

DMD Fast Forward. Published on November 3, 2020 as DOI: 10.1124/dmd.120.000115
This article has not been copyedited and formatted. The final version may differ from this version.

Figure 3. YM155 permeability across monkey BMECs (MBT-24H). (A) SLC35F2 mRNA expression in monkey BMECs. Conventional PCR analysis was conducted with nuclease free water and cDNA derived from isolated monkey brain microvascular endothelial cells constituting MBT-24H. (B) YM155 (0.1 μM) permeable amount at 2 and 4 h across monkey BMECs. The open squares and open circles represent A-to-B permeable amount of control and 1 mM famotidine-treated cells, respectively. (C) YM155 (0.1 μM) intracellular accumulation after 4 h permeability test. LLOQ indicates levels lower than the limit of quantification (0.02 pmol/well/4 h). The error bars represent the standard error of the mean (n = 3, mean ± SE). *p < 0.05 vs. permeable amount of control A-to-B direction. The experiments were conducted once using lot 24E50.

Figure 4. YM155 permeability across hiPS-BMECs and the effects of cationic compounds. (A) Immunoblotting of whole cell lysates of hiPS-BMECs confirmed their SLC35F2 protein expression, compared with hCMEC/D3 cells (D3) and undifferentiated hiPS cells (hiPS). (B) YM155 (0.1 μM) permeable amount across hiPS-BMECs. The open and closed squares represent the transport amount of A-to-B and B-to-A directions, respectively, and open circles represent A-to-B permeable amount with the 1 mM famotidine treatment. The bars represent YM155 permeable amount at 4 h. (C), (D) Calculated permeability coefficient (C) and intracellular accumulation (D) of YM155 with the treatment of various organic cations, 1 mM famotidine, 500 μM tetraethylammonium (TEA), 500 μM L-carnitine, 500 μM thiamine, and 1 mM L-arginine. Open and gray bars represent the data for the A-to-B direction, and the black bar represents the data for the B-to-A direction. The error bars represent the standard error of the mean (n = 3, mean ± SE). **p < 0.01, ***p < 0.001 vs. control value of A-to-B direction. The experiments were repeated at least twice.

Figure 5. Effects of SLC35F2 knockout on YM155 permeability across hiPS-BMECs. (A) Immunoblotting of whole cell lysates of hiPS-BMECs confirmed SLC35F2 knockout in

DMD Fast Forward. Published on November 3, 2020 as DOI: 10.1124/dmd.120.000115
This article has not been copyedited and formatted. The final version may differ from this version.

SLC35F2 sgRNA-treated hiPS-BMECs (KO), compared with green fluorescent protein (GFP) sgRNA-treated hiPS-BMECs (Con). (B), (C) hSLC35F2 localization in control (A) and SLC35F2 KO (B) hiPS-BMECs detected by confocal laser scanning microscopy. Green and blue signals represent SLC35F2 and nuclear staining, respectively. The upper sections illustrate the horizontal image and the lower sections illustrate the vertical image. Scale bars represent 10 μm. (D) 0.1 μM YM155 permeable amount of A-to-B transport across control hiPS-BMECs (open squares) and SLC35F2 KO hiPS-BMECs (closed squares), and B-to-A transport across control hiPS-BMECs (open triangles) and SLC35F2 KO hiPS-BMECs (closed triangles), respectively. The upper figure illustrates the permeable amount except for the data of control A-to-B transport. (E), (F) Calculated permeability coefficient (E) and intracellular accumulation (F) of 0.1 μM YM155 in control hiPS-BMECs (open bars) and SLC35F2 KO hiPS-BMECs (closed bars). The error bars represent the standard error of the mean (n = 4, mean ± SE). ***p < 0.001 vs. A-to-B transport in control hiPS-BMECs. The experiments were repeated at least twice.

Figure 6. Characterization of YM155 transport in the mouse BBB. (A)–(D) YM155 and pitavastatin brain distribution volumes were evaluated in an *in situ* brain perfusion test in mice. (A) Concentration dependency of YM155 brain distribution volume. (B) YM155 brain distribution volume in wild-type (WT) and *Slc35f2*$^{-/-}$ (KO) mice. (C) Effect of 1 mM famotidine (Fam) on YM155 brain distribution compared with inhibitor free conditions (Con) in WT mice. (D) Effects of 100 μM losartan (Los) and 100 μM naringin (Nar) on YM155 and pitavastatin brain distribution compared with inhibitor free conditions (Con) in WT mice. The vertical bars represent the standard error of the mean (n = 3–5, mean ± SE). *p < 0.05, **p < 0.01, ***p < 0.001 vs. control uptake. N.S. indicates $p \geq 0.05$. The experiments were repeated at least twice.

DMD Fast Forward. Published on November 3, 2020 as DOI: 10.1124/dmd.120.000115
This article has not been copyedited and formatted. The final version may differ from this version.

Tables

Table 1. Kinetic parameters of YM155

The kinetic parameters of YM155 uptake in hSLC35F2-HEK293 and mSLC35F2-HEK293 cells (**Supplementary Figure 1D**) and parental hCMEC/D3 cells (**Figure 2B**). The values represent mean ± computer-calculated SD. The experiments were repeated at least twice.

	$K_{m,\ app}$ (μM)	$V_{max,\ app}$ (pmol/min/mg protein)	P_{dif} (μL/min/mg protein)
hSLC35F2	0.310 ± 0.038	15.2 ± 1.1	2.41 ± 0.21
mSLC35F2	1.55 ± 0.36	97.1 ± 20.9	2.47 ± 1.68
hCMEC/D3	0.573 ± 0.166	1.74 ± 0.35	0.277 ± 0.046

DMD Fast Forward. Published on November 3, 2020 as DOI: 10.1124/dmd.120.000115
This article has not been copyedited and formatted. The final version may differ from this version.

Table 2. Effects of organic cations on YM155 uptake in PC-3 and hCMEC/D3 cells.

We determined 5 min YM155 (0.1 μM) uptake mediated by SLC35F2 in control PC-3 or hCMEC/D3 cells in the absence and presence of the test compounds. Values represent mean ± SE (n = 3–4). TEA: tetraethylammonium. *p < 0.05, **p < 0.01 vs. control. N.D. indicates no data. The experiments were repeated at least twice.

Conditions/Compounds	conc.	% of control YM155 uptake	
		PC-3	hCMEC/D3
Control	free	100 ± 6	100 ± 8
SLC35F2 knockout		10.3 ± 1.0 **	N.D.
L-carnitine	1 mM	125 ± 14 **	120 ± 4 *
TEA		83.4 ± 1.8	64.2 ± 4.9 **
varenicline		76.4 ± 3.0 **	84.3 ± 10.4
famotidine		16.4 ± 1.8 **	15.1 ± 0.6 **
tramadol		13.0 ± 1.0 **	32.6 ± 5.6 **
clonidine		9.06 ± 0.47 **	21.9 ± 1.3 **
diphenhydramine		5.65 ± 0.32 **	12.4 ± 0.7 **
pyrilamine		5.46 ± 0.97 **	14.1 ± 1.3 **
imipramine		5.36 ± 0.34 **	34.4 ± 2.5 **
verapamil	100 μM	5.11 ± 0.28 **	27.0 ± 6.1 **
quinidine		3.22 ± 0.51 **	15.1 ± 0.6 **

DMD Fast Forward. Published on November 3, 2020 as DOI: 10.1124/dmd.120.000115
This article has not been copyedited and formatted. The final version may differ from this version.

Table 3. Half-maximal inhibitory concentration (IC_{50}) against YM155 uptake mediated by SLC35F2.

Values represent IC_{50} of the compounds against 5 min YM155 (0.1 μM) uptake mediated by SLC35F2 in control PC-3 cells. Detailed data is presented in **Supplementary Figure 3**. Values represent mean ± computer-calculated SD. The experiments were repeated at least twice.

Compound	IC_{50} (μM)
Famotidine	160 ± 28
Pyrilamine	101 ± 27
Clonidine	77.7 ± 14.6
Diphenhydramine	65.7 ± 6.8
Imipramine	17.2 ± 5.2
Quinidine	4.01 ± 0.73

Figure 1

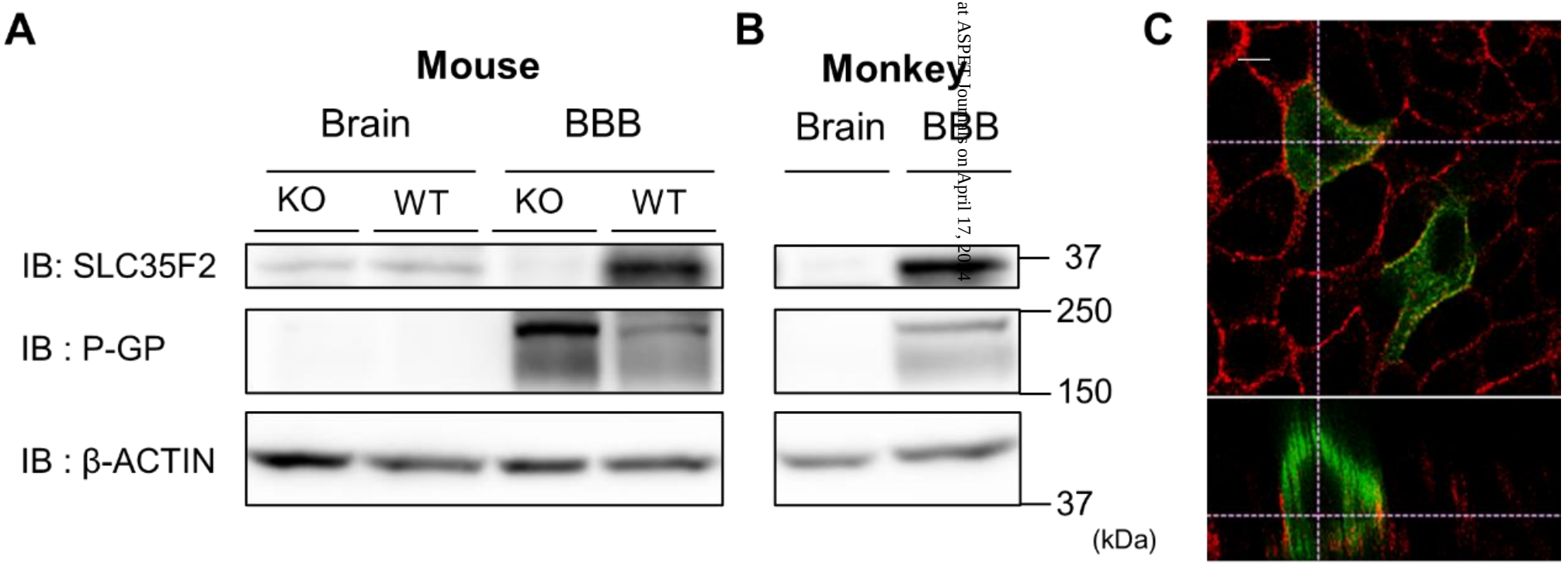

Figure 2

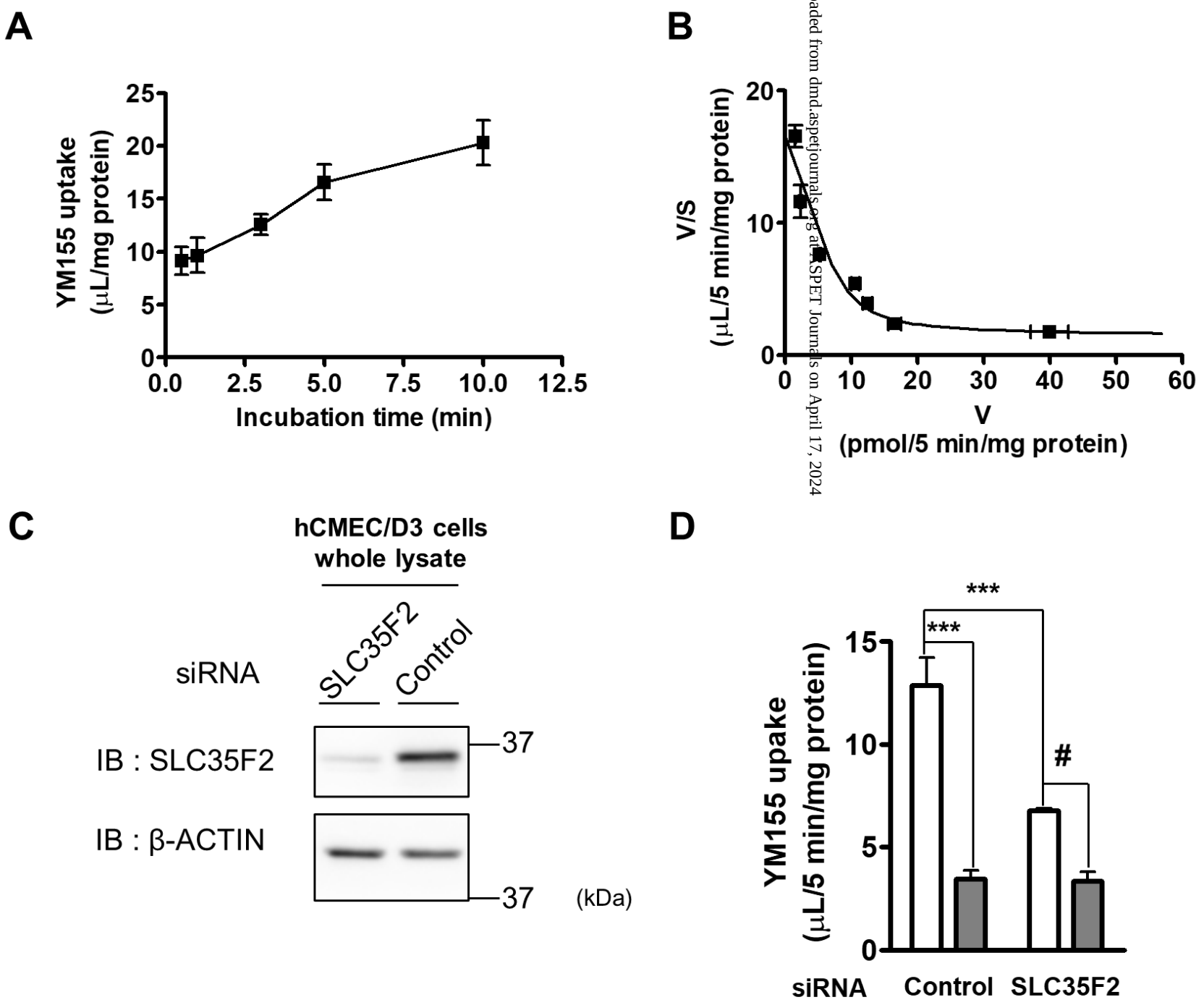

Figure 3

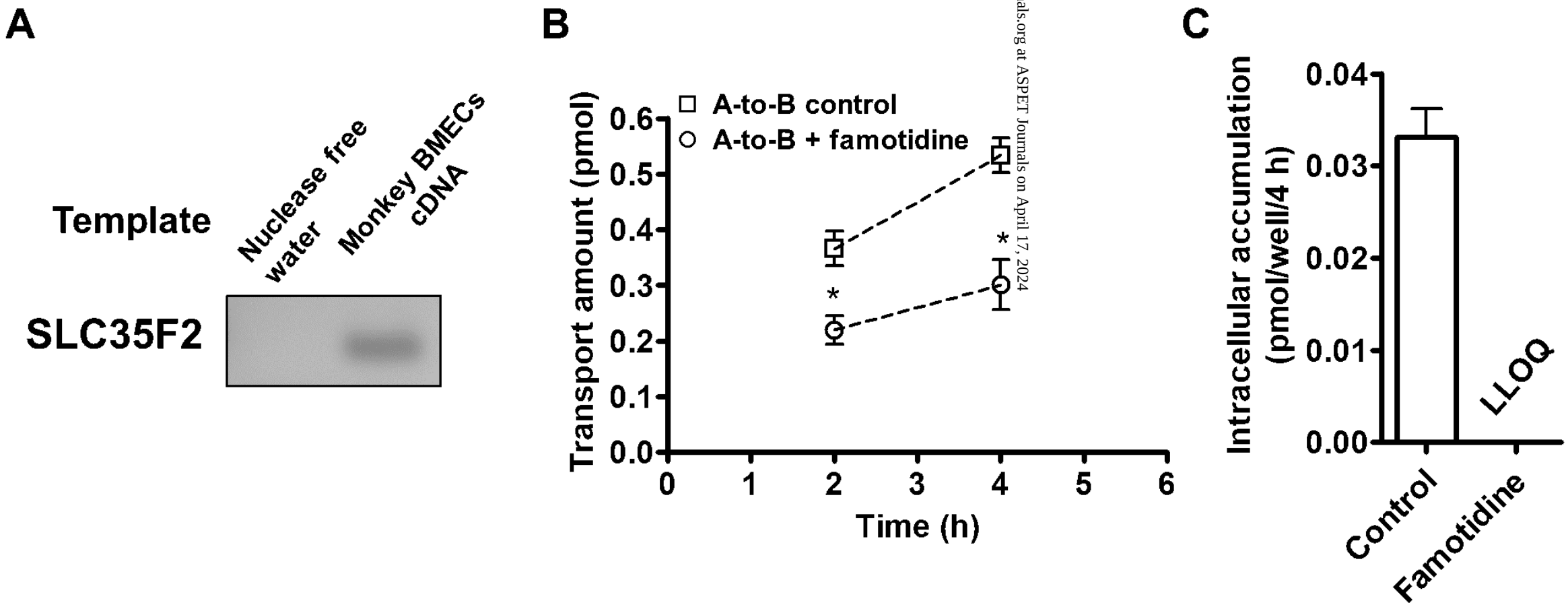

Figure 4

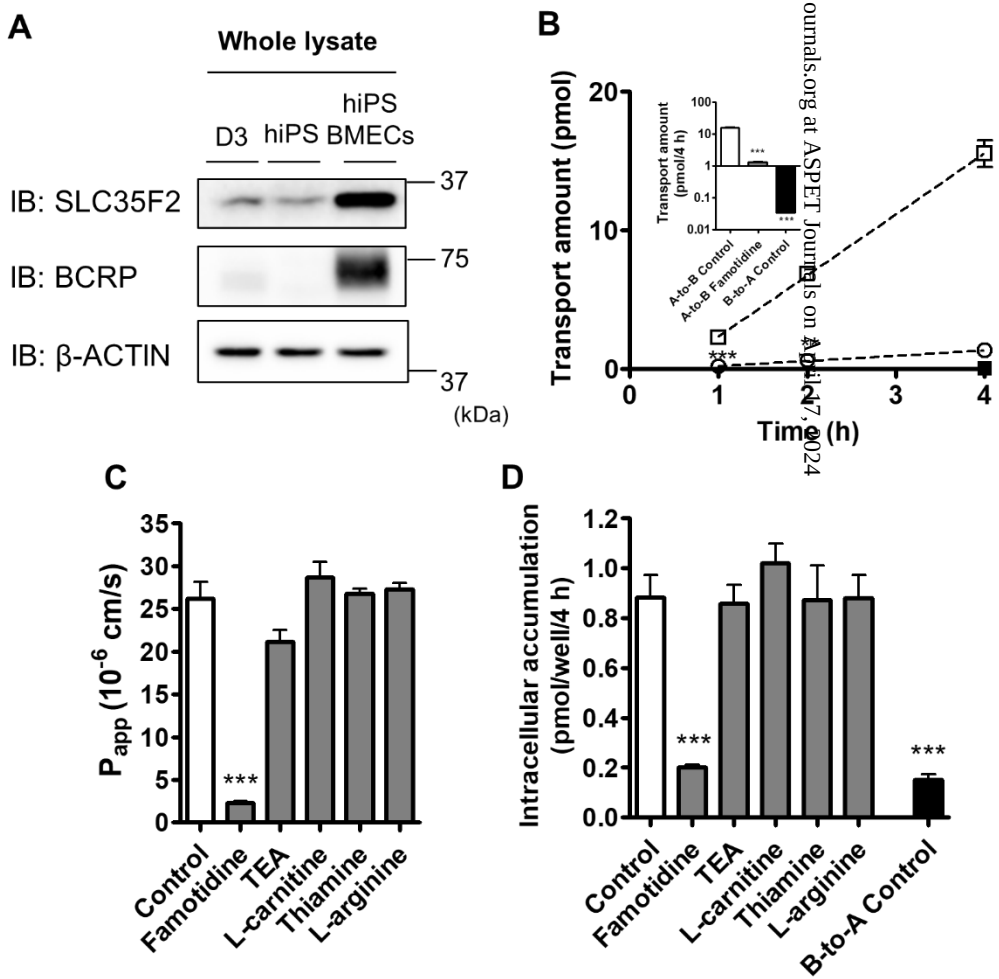

Figure 5

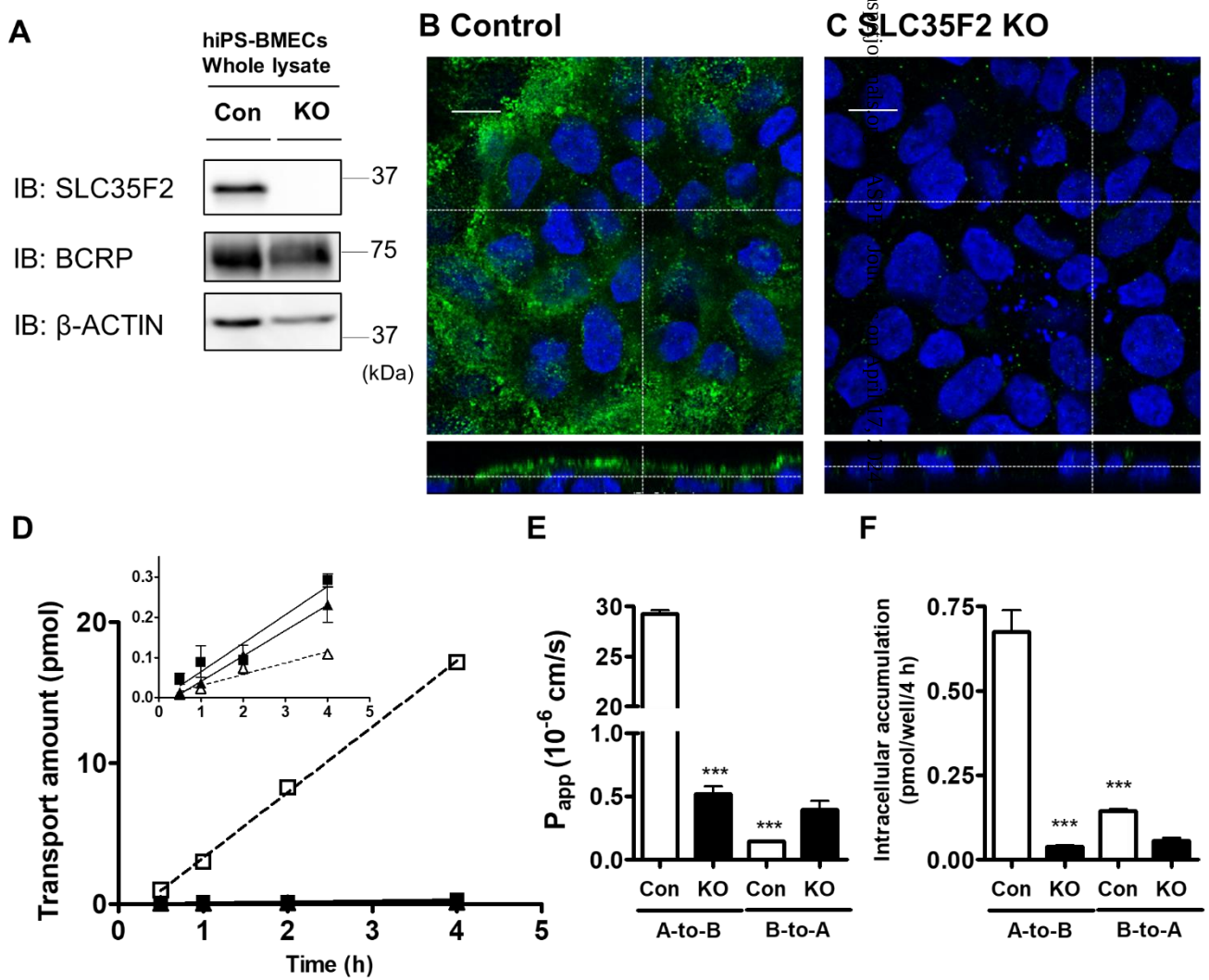

Figure 6